

See discussions, stats, and author profiles for this publication at: <https://www.researchgate.net/publication/267157909>

DNA Recognition with Polycyclic-Aromatic-Hydrocarbon-Presenting Calixarene Conjugates

ARTICLE in EUROPEAN JOURNAL OF ORGANIC CHEMISTRY · DECEMBER 2014

Impact Factor: 3.07 · DOI: 10.1002/ejoc.201403050

READS

82

9 AUTHORS, INCLUDING:



Antonio Rescifina

University of Catania

106 PUBLICATIONS 1,586 CITATIONS

[SEE PROFILE](#)



Ugo Chiacchio

University of Catania

202 PUBLICATIONS 2,511 CITATIONS

[SEE PROFILE](#)



Carmen Talotta

Università degli Studi di Salerno

27 PUBLICATIONS 192 CITATIONS

[SEE PROFILE](#)



Carmine Gaeta

Università degli Studi di Salerno

72 PUBLICATIONS 834 CITATIONS

[SEE PROFILE](#)

DNA Recognition with Polycyclic-Aromatic-Hydrocarbon-Presenting Calixarene Conjugates

Antonio Rescifina,^{*[a]} Chiara Zagni,^[a] Placido G. Mineo,^[b,c] Salvatore V. Giofrè,^[d] Ugo Chiacchio,^[a] Stefano Tommasone,^[e] Carmen Talotta,^[e] Carmine Gaeta,^[e] and Placido Neri^{*[e]}

Dedicated to C.I.N.M.P.I.S. on the occasion of its 20th anniversary

Keywords: Intercalations / Calixarenes / Heterocycles / Polycycles / DNA recognition

New calix[4]arene conjugates that present polycyclic aromatic hydrocarbons (PAHs) at their *exo* rims have been synthesized by esterification of a cone-shaped calix[4]arene-dicarboxylic acid with *trans*- or *cis*-pyrenylisoxazolidinyl alcohols prepared by a 1,3-dipolar cycloaddition methodology. The *in vitro* cytotoxic activities of all compounds were

evaluated with three different human tumor cell lines, and the most potent one reached an IC₅₀ of 95 nM. The different biological activities of the synthesized compounds were explained by docking and circular dichroism studies, which evidenced their intercalating abilities from the DNA minor groove.

Introduction

Since the discovery of DNA as the main driving force in tumorigenesis, it has become one of the principal intracellular targets in cancer chemotherapy.^[1] Research in this area has disclosed a range of DNA-recognizing molecules, which act as antitumor agents. DNA-interacting drugs are either intercalators, which bind to DNA by intercalating between the stacked base pairs and, thereby, distort its backbone conformation, or groove binders, which fit into the DNA minor groove and only slightly perturb the DNA structure.^[2]

DNA intercalators are usually polycyclic aromatic hydrocarbons (PAHs), which bind reversibly to DNA by intercal-

ation of a flat aromatic system between base pairs and form DNA-drug complexes stabilized by π-π and van der Waals interactions, hydrogen bonding, hydrophobic effects, or charge-transfer forces. This intercalation results in structural changes that cause the unwinding of the DNA helix and the extension of the DNA chain by one base pair. Such modifications can prevent RNA and DNA polymerase from binding to the DNA and affect the initiation of transcription and replication; this results in the inhibition of the replication process and thence cell death.^[3]

Recently, several studies in this field have focused on bisintercalating compounds, which generally consist of two aromatic units connected by a linker that is chosen to modify binding affinity or specificity.^[4] Bisintercalators exhibit increased binding affinities, which can lead to improved cytotoxicity, the formation of more DNA adducts (which reduces the effectiveness of DNA-repairing proteins), and slower dissociation rates than those of the corresponding monomers.^[5] Several dimeric DNA intercalators, such as bisnaphthalimides (**1**), bisacridinecarboxamides (**2**), and bisimidazoacridones (**3**, Figure 1),^[5] have been developed as potential anticancer drugs.^[6]

In recent years, we have synthesized a series of PAH-isoxazolidinyl derivatives in which an isoxazolidine ring is linked to a planar aromatic anthracene, phenanthrene, or pyrene system.^[7] Binding studies have shown that all of these derivatives bind to some extent to DNA by intercalation and have IC₅₀ values in the low micromolar range; compounds **4** (Figure 1) are representative of the first gen-

[a] Dipartimento di Scienze del Farmaco, Università di Catania, V.le A. Doria 6, 95126 Catania, Italy
E-mail: arescifina@unict.it
<http://www.dsf.unict.it>

[b] Dipartimento di Scienze Chimiche and I.N.S.T.M. UdR of Catania, Università di Catania, Viale A. Doria 6, 95125 Catania, Italy

[c] CNR-IPCF Istituto per i Processi Chimico Fisici, Viale Ferdinando Stagno D'Alcontres 37, 98158 Messina, Italy

[d] Dipartimento di Scienze del Farmaco e dei Prodotti per la Salute, Università di Messina, Via S. S. Annunziata, 98168 Messina, Italy

[e] Dipartimento di Chimica e Biologia, Università di Salerno, Via Giovanni Paolo II 132, 84084 Fisciano (Salerno), Italy
E-mail: neri@unisa.it
http://www.unisa.it/dipartimenti/dip_chimica_e_biologia/index

Supporting information for this article is available on the WWW under <http://dx.doi.org/10.1002/ejoc.201403050>.

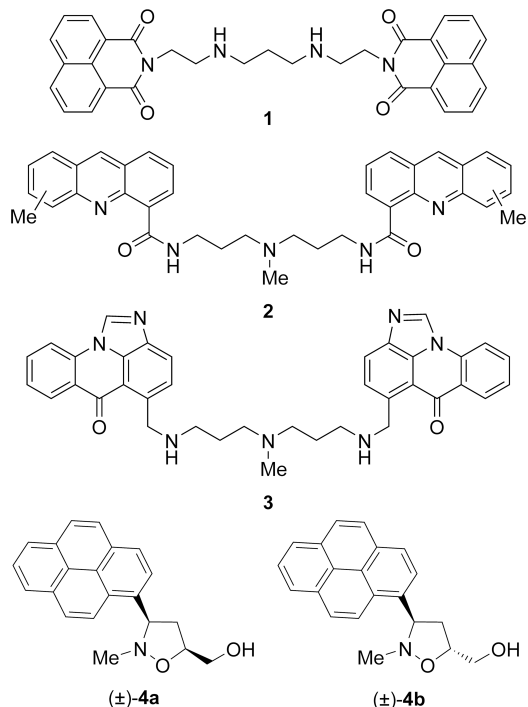


Figure 1. DNA intercalators.

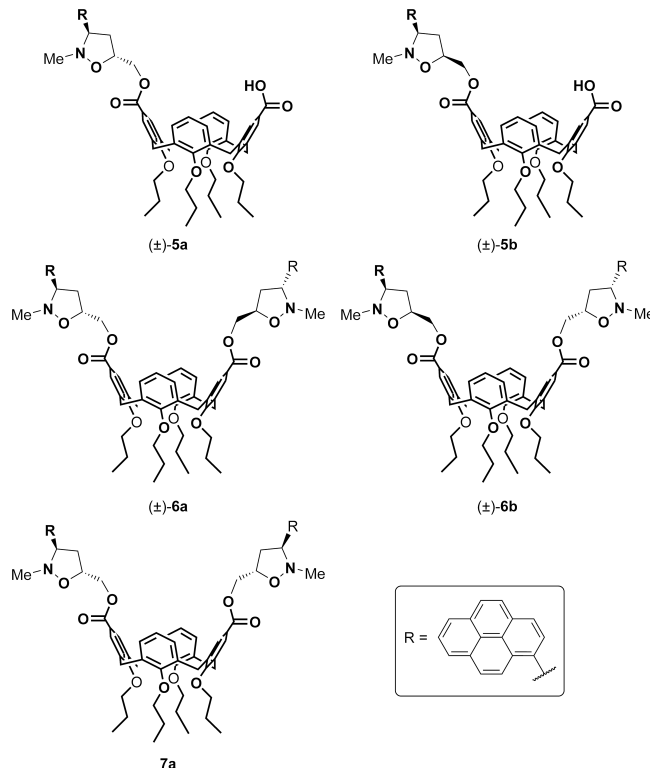


Figure 2. PAH-presenting calix[4]arene conjugates.

eration of our PAH-isoxazolidinyl derivatives, and **4a** has an IC₅₀ of 112 μ M for the molt-3 cell line.^[7a]

Calix[4]arenes consist of a cavity-containing three-dimensional aromatic scaffold with a great synthetic versatility,^[8] which allows the introduction of functionalities at both the upper (or *exo*) and lower (or *endo*) rims.^[9] In recent decades, calixarene hosts have shown interesting interactions with biological targets^[10] such as enzymes,^[11] growth^[12] and transcriptional^[13] factors, and membrane proteins.^[14] In 2005, we reported calix[4]arenes bearing tetrapeptides at the *exo* rim (peptidocalixarenes)^[10b] that showed *in vitro* inhibition activities towards transglutaminase enzymes,^[11c] and Hamilton and co-workers reported calixarenes bearing cyclic peptides at the *exo* rim as platelet-derived growth factor (PDGF) binders, which showed anti-cancer and antiangiogenic activity.^[12] Recently, we have shown that arylamidocalix[4]arene derivatives bearing large hydrophobic groups at the *exo* rim are effective as histone deacetylase inhibitors (HDACi).^[11b]

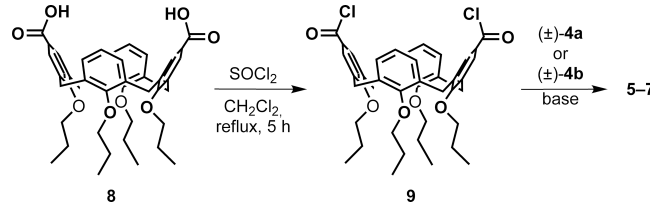
Regarding calixarene derivatives as DNA-binding agents, Schrader recently reported calixarene dimers that strongly prefer the DNA major groove.^[15] Ungaro and co-workers showed that calix[4]arenes bearing cationic guanidinium groups at the *exo* or *endo* rim could bind to DNA and perform cell transfection.^[16]

On the basis of these interesting results, we have now designed and synthesized calix[4]arene/pyrenylisoxazolidine conjugates **5–7** (Figure 2) in which one or two pyrenylisoxazolidine moieties are linked at the calix[4]arene *exo* rim as potential DNA intercalators and suitable tools for cooperative DNA complexation.^[17]

Results and Discussion

Chemistry

The key step in the synthesis of PAH-calixarenes **5–7** was the ester bond formation between the carboxyl groups of the known calix[4]arenedicarboxylic acid **8**,^[18] blocked in the cone conformation, and the *trans*- or *cis*-pyrenylisoxazolidinyl alcohols (\pm)-**4a** and (\pm)-**4b** (Scheme 1).^[7a] In particular, diacid **8** was converted into the corresponding diacyl chloride **9** and then coupled with the pertinent racemic alcohol (\pm)-**4a** or (\pm)-**4b** with pyridine or triethylamine as base. After a standard workup, the two expected disubstituted derivatives, namely, the racemic pair with C_2 symmetry **6a/b** and the *meso* compound with C_s symmetry **7a**, were isolated by silica gel column chromatography together with a certain amount of the monosubstituted **5a/b**.



Scheme 1. Synthesis of pyrenylisoxazolidinylcalix[4]arene conjugates **5–7**.

The ESI(+) mass spectra of **5–7** confirmed the presence of one or two pyrenylisoxazolidinyl moieties at their *exo*-rims. Regarding the stereochemistry, the C_2 or C_s symmetry of the bis-derivatives **6–7** was assigned on the basis of the

number of NMR resonances. Thus, for example, the ^1H NMR spectrum (400 MHz, 298 K, CDCl_3) of **6a** showed two sets of signals for the two C_2 -related $\text{OCH}_2\text{CH}_2\text{CH}_3$ chains. Two OCH_2 triplets were present at $\delta = 3.69$ ($J = 6.3$ Hz, 4 H) and 4.04 ppm ($J = 7.6$ Hz, 4 H), and two terminal CH_3 triplets were found at $\delta = 0.91$ and 1.07 ppm (6 H each). In addition, the 2D heteronuclear single quantum coherence (HSQC) spectrum showed two cross-peaks at $\delta = 3.69/76.9$ and 4.04/76.7 ppm (see inset in Figure S11) relative to a direct C–H correlation between the two above-described OCH_2 protons and the two pertinent carbon resonances. Analogously, the COSY-45 spectrum revealed the presence of two ArCH_2Ar AX systems at $\delta = 3.17/4.39$ and 3.20/4.42 ppm. Clearly, all these data confirm the C_2 symmetry of (\pm) -**6a** and rule out the alternative C_s meso stereoisomer.

In a similar way, the C_s symmetry of the *meso* derivative **7a** was evident from its ^1H NMR spectrum (400 MHz, 298 K, C_6D_6 , inset in Figure S12), which showed three OCH_2 signals at $\delta = 3.86$, 3.70, and 3.69 ppm (4 H, 2 H, and 2 H, respectively) indicative of the presence of a σ_h symmetry plane bisecting the unsubstituted aromatic rings. In accordance with this symmetry, the ^{13}C NMR spectrum of **7a** (63 MHz, 298 K, CDCl_3) showed three signals for the aromatic oxygenated carbon atoms at $\delta = 162.1$, 155.9, and 155.8 ppm.

The C_1 structure of the monosubstituted conjugates (\pm) -**5a** and (\pm) -**5b** was readily evident by the complexity of their NMR spectra, which were fully consistent with the structure lacking any symmetry element. For example, the COSY spectrum of **5b** (250 MHz, 298 K, CDCl_3) revealed the presence of four AX systems for the ArCH_2Ar groups at $\delta = 3.10/4.53$ (2 H), 3.18/4.45 (2 H + 2 H, overlapped), and 3.18/4.40 ppm (2 H), which are consistent with the C_1 structure of **5b**. Analogously, the asymmetric structure of **5a** was confirmed by the presence of four distinct doublets for the pseudoequatorial ArCH_2Ar protons in its ^1H NMR spectrum (400 MHz, 298 K, CDCl_3) in the $\delta = 3.18$ –3.26 ppm region.

Biology

To investigate the effects of the new potential DNA binders, we evaluated their ability to inhibit the proliferation of cancer cells *in vitro*. Thus, three different human tumor cell lines were cultured: FTC133 (follicular thyroid carcinoma, lymph node metastasis), 8305C (undifferentiated thyroid carcinomas), and U87MG (glioblastoma). After 24 h of incubation with **4**–**7**, the cell growth rates were evaluated by 3-(4,5-dimethylthiazol-2-yl)-2,5-diphenyltetrazolium bromide (MTT) reduction assays, which are based on the ability of mitochondrial dehydrogenase enzymes from viable cells to cleave the tetrazolium rings. The results, shown in Table 1, are expressed as IC_{50} values (the concentration of compound at which 50% of cells are viable). All calixarenes were prepared as clear dimethyl sulfoxide (DMSO) stock solutions, but they partially precipitated

(principally at 10 and 100 μM concentrations) when added to the cell culture medium. This was especially crucial for the bispyrenyl calixarenes **6** and **7**. Thus, all of the IC_{50} values probably result from slightly lower ligand concentrations with respect to those effectively used, as also reported for slightly soluble dimeric calixarenes.^[15b] Among the tested compounds, **5b** was the most cytotoxic and exhibited an IC_{50} value of 95 nm toward FTC133 cells. Compound **6b** was ca. 580-fold less cytotoxic than **5b** with an IC_{50} value of 55 μM and 10-fold less potent than the isoxazolidines **4a** and **4b**, which had IC_{50} values of 5.52 and 5.88 μM , respectively. Surprisingly, **5a**, which is the *trans* isomer of **5b**, exhibited low cytotoxicity and had an IC_{50} value higher than 100 μM . A lack of activity at concentrations below 100 μM was also found for **6a**, **6b**, and **7a**. These results show that stereochemistry plays an important role in the activity of plausible monointercalators, as the *cis* isomer **5b** exhibited better activity than the *trans* isomer **5a** toward the cell lines tested. In contrast, the conceivable bisintercalators did not show the promising results we expected. This can likely be attributed, in part, to a deprotonation of the carboxylic functionality of **5b** under physiological conditions, which would increase its solubility and facilitate the insertion into the nucleus.

Table 1. Cytotoxicity of **4**–**7** expressed as IC_{50} [μM]^[a] and determined by MTT assay.^[b]

Compound	FTC133	8305C	U87MG
4a	5.52	–	5.36
4b	5.88	–	5.55
5a	>100	>100	>100
5b	0.095	0.130	57
6a	>100	>100	>100
6b	55	55	>100
7a	>100	>100	>100

[a] Each value was determined from quadruplicate samples by nonlinear regression analysis. [b] The cells were exposed under optimal culture conditions in 96-well plates to five concentrations of the compound (0.01, 0.1, 1.0, 10, 100 μM) or control medium for 24 h before determination of the cellular metabolic activity by an MTT bioreduction assay.

Moreover, we must also take into account that this cell growth inhibition might not only be reached by DNA complexation of substituted calixarenes inside tumor cells. Calixarenes are able to self-assemble inside the cell membrane and alter the membrane potential as well as the ion flux across the double layer.^[14b] In consideration of this hypothesis, membrane potential measurements along with cell cycle analyses are in progress to shed more light on this aspect.^[19]

However, the role of the calixarene moiety in the biological activity is evident, because **5b** is 58-fold more potent than the precursor **4a**, and its activity cannot be imputable to a mere hydrolysis of the ester functionality.

Circular Dichroism

To gain a deeper insight into the changes of polynucleotide properties induced by PAH–calixarene binding and to

prove – or disprove – the postulated intercalation between base pairs, we studied the behavior of **5b** and **6b** on interaction with the poly(dA)–poly(dT) duplex [duplex of poly(deoxyadenylic acid) and poly(deoxythymidylic acid)] by CD.

The CD spectrum of poly(dA)–poly(dT) in the B form displays two conserved peaks at $\lambda = 248$ and 260 nm; the first one is negative and is due to right-handed helicity, whereas the second one is positive and is due to base stacking.^[20]

The CD titration spectra of poly(dA)–poly(dT) duplex in the presence of increasing amounts of **5b** are shown in Figure 3. Increasing concentrations of **5b** led to decreases in the intensities of the $\lambda = 248$ and 260 nm signals without any shift in their positions and a concomitant appearance of an increasing, positive, induced CD (ICD) signal at 342 nm. These results are consistent with an intercalative binding of the pyrene moiety with the tethered calixarene located along the groove. Moreover, an isodichroic point at $\lambda = 253$ nm is well defined for the entire titration course, which suggests that there is only one mode of binding in solution, that is, there are only two DNA absorbing species present, namely, the free species and the species bound to the calix[4]arene/pyrenylisoxazolidine conjugate.^[21]

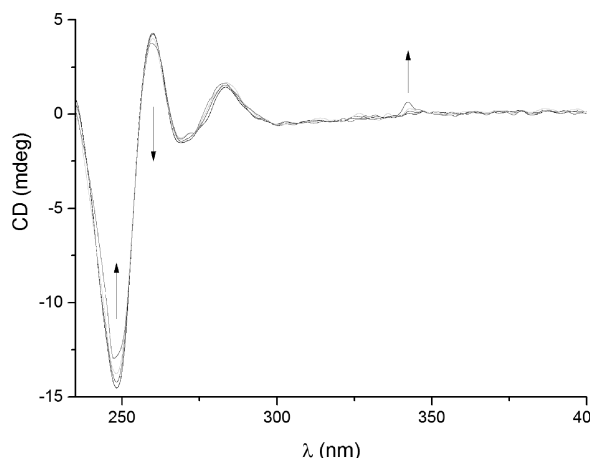


Figure 3. CD spectra of the **5b**-poly(dA)–poly(dT) system at 25 °C. [poly(dA)–poly(dT)] = 19.7 μM in base pair and [5b] = 0–32 μM.

In particular, the changes in the intrinsic CD spectrum of the negative signal of the poly(dA)–poly(dT) duplex reflect the diminished helicity (helix unwinding), because intercalation enables the sugar–phosphodiester backbone to span the bound intercalator and still maintain the link between the two flanking base pairs and the extent of base stacking;^[22] this unwinding also agrees with a concomitant groove widening to accommodate the sterically demanding calixarene portion.^[15b] The observed reduction in the positive dichroic signal is likely due to a conformational change from a more B-like to a more C-like structure.^[21,23] Both of these behaviors have recently been observed for molecules for which the ability to behave as DNA intercalators was confirmed by the application of more instrumental techniques.^[24] From these results, it can be concluded that **5b** is able to unwind DNA without increasing its length, contrar-

ily to what is predicted by the classical intercalation model in which an increment of both negative and positive signals is observed.^[25] This last model is preferentially applicable when the ligand is a pure intercalating agent without a pendant chain that can interact with the groove, as for simple pyrenyl derivatives.^[26]

Finally, the small positive ICD signal at $\lambda = 342$ nm proves the intercalation phenomenon and contemporarily establishes the geometry of the ligand: the ICD sign is in accord with the pyrene moiety perpendicular to the DNA axis with its long direction parallel to the base-pair long axis.^[26a,27] Although **5b** and **6b** are chiral species, it should be noted that they are racemic mixtures. These systems show silent CD spectra, which indicates that the observed ICD phenomenon is genuine.

The **6b**-poly(dA)–poly(dT) system showed similar CD spectra but with reduced changes in intensity.

These CD experimental data are qualitatively in accord with those obtained in silico. The performed docking of **5b** with poly(dA)–poly(dT) dodecamer gave the following binding energies: −9.92 and −6.43 kcal/mol for intercalation from the minor and the major groove, −6.57 and −5.72 kcal/mol for binding along the minor and major groove. These data are in accord with those obtained with (dA–dT)₂ and (dG–dC)₂ dodecamers (Table 2).

Table 2. Calculated binding energies [kcal/mol] for **4** and **5–6** intercalated or groove-bound to (dA–dT)₂ and (dG–dC)₂ dodecamers after 5 ns of MD simulation.

Compound	(dA-dT) ₂ dodecamer	
	From major groove	From minor groove
4a (intercalated)	−9.68	−9.39
4b (intercalated)	−9.11	−9.03
5a (intercalated)	−6.53	−8.83
5b (intercalated)	−6.694	−10.19
6a (intercalated)	−9.22 ^[a] , −7.36 ^[b]	−9.81
6b (intercalated)	−11.16 ^[a] , −8.13 ^[b]	−15.51
5a (groove-bound)	−4.66	−7.79
5b (groove-bound)	−4.35	−8.16
6b (groove-bound)	−8.35	−8.79
(dG-dC) ₂ dodecamer		
	From major groove	From minor groove
4a (intercalated)	−9.35	−9.23
4b (intercalated)	−9.28	−9.09
5a (intercalated)	−6.76	−7.33
5b (intercalated)	−8.91	−10.88
6a (intercalated)	−8.48	−9.05
6b (intercalated)	−10.55	−13.09
5a (groove-bound)	−5.13	−7.54
5b (groove-bound)	−4.41	−8.65
6b (groove-bound)	−8.15	−8.98

[a] After 1 ns of MD. [b] After 5 ns of MD.

Molecular Modeling

To confirm and rationalize the observed biological and CD results and gain more insight into the intercalation modality of **5b** and the failure of **5a**, the supramolecular complexes of the synthesized compounds with DNA have been investigated by a molecular modeling methodology. Al-

though the obtained compounds are racemates, we have already demonstrated that compounds with a (3*R*) configuration (for the isoxazolidine ring) possess the best intercalating properties.^[7c] Thus, all molecular docking calculations were performed for (3*R*) stereoisomers.

The adopted molecular modeling template consists of the following five steps: (1) Poly(dA-dT)₂, poly(dG-dC)₂, and poly(dA)-poly(dT) were simulated as double-stranded dodecamer fragments, (dA-dT)₂, (dG-dC)₂ and poly(dA)-poly(dT), respectively. They were constructed in the B-DNA conformation with the nucleic acids macro implemented in the YASARA software^[28] and minimized with the Amber03 force field,^[29] which is one of the most accurate force fields for DNA minimization and molecular dynamics (MD) simulations and ensures DNA stability until 25 ns.^[30] (2) The simulations for the intercalation between paired nucleobases of all compounds bound to dodecamers were performed by the docking methodology.^[31] Firstly, the compound was manually inserted into the middle base-step of each fragment from the minor groove or the major one (for monointercalations between the sixth and seventh base pairs and for bisintercalation between the fifth and sixth as well as the seventh and eighth base pairs, simultaneously). Although the atom positions of the compound were fixed, the remaining molecules were minimized to make the free fragment adjust to suitably accommodate the ligand. (3) To obtain the best and most reliable docking results, a coarse docking simulation was first performed for each complex by applying the Lamarckian genetic algorithm (LGA) implemented in AutoDock 4.2.5.1,^[32] which has been recently demonstrated to accurately reproduce the complex crystallographic structures of a collection of DNA-binding small ligands.^[33] (4) The best ligand position was further subjected to an MD simulation of 5 ns in a physiological environment (pH = 7.2, H₂O, NaCl 0.9%) to allow the ligand to be better accommodated in the pocket and model the interactions with the groove. (5) Finally, each ligand was well docked by the LGA with the system obtained by MD. Under physiological conditions, the carboxylic acid moiety in ligands **5** is completely dissociated; therefore, only their carboxylate form was considered for all molecular modeling studies.

We also considered the possibility that the complexation of **5–6** with DNA may occur by binding along the grooves. This last task was performed similarly to the above-described procedure but with step (2) eliminated and step (3) substituted with a blind docking procedure.^[34]

The calculated binding energies of the above docking study, after 5 ns of MD simulation, are summarized in Table 2 with the exception of that of the **5b**-poly(dA)-poly(dT) system, which is reported in the CD section.

The new compounds **5–7** (except for **5b**) can act as mono- or bisintercalators that interact preferentially with AT base pairs and penetrate into the DNA double helix exclusively from the minor groove and establish van der Waals interactions between the two pyrene rings and the nucleotidic base pairs; the calixarene moiety principally plays a linker role. Intercalation from the major

groove and minor or major groove binding can be ruled out on the basis of their lower (less negative) binding energies.

The lower cytotoxic activity of the *trans* stereoisomer **5a** compared to that of the *cis* one **5b** is probably imputable to the steric hindrance of the *N*-Me group of the isoxazolidine ring. The graphical representations of **5a** and **5b** intercalated from the minor groove in the (dA-dT)₂ dodecamer fragment are presented in Figure 4: it is evident that the isoxazolidine *N*-methyl group in the *trans* isomer **5a** (Figure 4, left) points directly towards the crowded inner groove base pairs, whereas the same methyl group in the *cis* isomer **5b** (Figure 4, right) faces outward and produces a lower encumbrance. Moreover, in the **5b**-(dA-dT)₂ dodecamer system, the long axis of the pyrene moiety is almost parallel to that of the upper base-pair conjoining line.

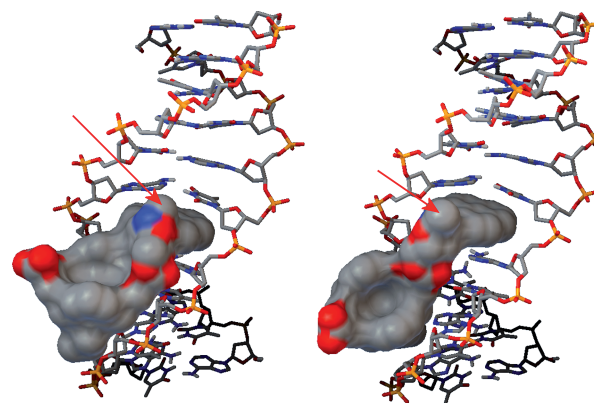


Figure 4. Plots representing **5a** (left) and **5b** (right) intercalated into the (dA-dT)₂ dodecamer from the minor groove. The red arrows indicate the *N*-Me group of the isoxazolidine ring.

Compounds **6a** and **6b** behave as bisintercalators, and the calculated binding energy of -15.51 kcal/mol for the latter presupposes a very tight interaction with DNA that should theoretically lead to a biological activity in the sub-micromolar range. Nevertheless, the registered IC₅₀ value of 55 μm could be imputable to the low solubility.

Interestingly, both **6a** and **6b** can only act as monointercalators when they enter from the major groove of poly(dA-dT)₂; this behavior was explained by examining the MD simulation trajectories. After the first nanosecond, both compounds **6** are perfectly bisintercalated into the dodecamer; this is shown in Figure 5 (left) for **6b**. During the subsequent 1.3 ns, one pyrene moiety deintercalates and becomes perpendicular to the calixarene *exo* rim. At the end of the 5 ns simulation, **6** is monointercalated with the main axis of the intercalated pyrene ring perpendicular to the base-pair conjoining line, and the pocket between the deintercalated base pairs is closed (Figure 5, right). However, the binding energies for these two MD periods (1 and 5 ns, Table 2) are smaller than those obtained for the insertion of the compounds from the minor groove. For the interaction with the (dG-dC)₂ dodecamer, this trend is not observed, and the bisintercalate complexes are stable up to 5 ns of MD simulations.

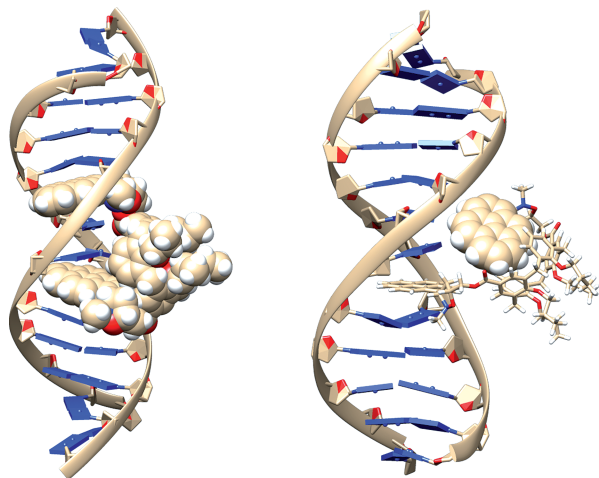


Figure 5. Plot representing **6b** intercalated into the (dA–dT)₂ dodecamer from the major groove. After 1 ns of MD simulation, the two pyrene moieties are both intercalated (left); after 5 ns, only one pyrene moiety is intercalated, and the other is completely deintercalated and the corresponding pocket is closed (right).

Finally, the arrangement of **5b** into the pocket of poly(dA)–poly(dT) from the minor groove is depicted in Figure 6; it is evident that the long axis of the pyrenyl moiety is parallel to the long axis of the dyad bases, in good agreement with the ICD signal at $\lambda = 342$ nm (Figure 3).

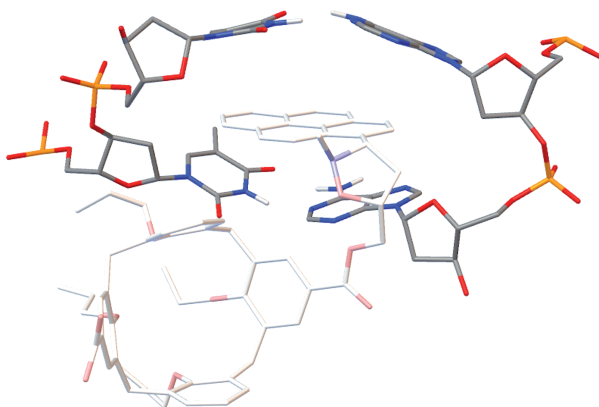


Figure 6. Plot representing **5b** intercalated into the poly(dA)–poly(dT) dodecamer from the minor groove.

Conclusions

We have reported new PAH-presenting calix[4]arene conjugates in which one or two pyrenylisoxazolidine moieties are linked at the calix[4]arene *exo* rim to act as DNA mono- and bisintercalating agents. They were readily synthesized by esterification of a cone-shaped calix[4]arenedicarboxylic acid with *trans*- or *cis*-pyrenylisoxazolidinyl alcohols, which were prepared by a 1,3-dipolar cycloaddition methodology. All of the obtained compounds were tested for their in vitro cytotoxic activity toward three different human tumor cell lines, and the most-potent one showed an IC₅₀ of 95 nm toward the follicular thyroid carcinoma, lymph node metas-

tasis (FTC133) cells. A 58-fold increase in activity was observed compared to that of the simple pyrenylisoxazolidinyl alcohols. Docking and CD studies have clearly indicated that these compounds can efficiently complex to DNA by intercalation between base pairs through an approach to the DNA double helix from its minor groove; they exhibit strong selectivity for the AT nucleobases, except for **5b**, which shows a slight preference for the GC base pairs. In light of these studies, a rationale is provided to explain the different biological activities observed. Undoubtedly, a crucial role is played by the low solubility of the PAH-presenting calix[4]arene conjugates in the cell culture medium. Therefore, future efforts will be directed at addressing this issue to obtain new DNA-intercalating agents with improved antitumor activity.

Experimental Section

General Methods: All chemicals were reagent grade and were used without further purification. Anhydrous solvents were purchased from Aldrich. Melting points were determined with a Kofler apparatus. Elemental analyses were performed with a Perkin–Elmer elemental analyzer. ESI(+) MS measurements were performed with a Micromass Bio-Q triple quadrupole mass spectrometer equipped with an electrospray ion source, and a mixture of H₂O/CH₃CN (1:1) and 5% HCOOH was used as solvent. Flash chromatography was performed with Merck silica gel (60, 40–63 µm). Reaction temperatures were measured externally; reactions were monitored by TLC with Merck silica gel plates (0.25 mm), which were visualized by UV light and spraying with H₂SO₄/Ce(SO₄)₂. NMR spectra were recorded with a Bruker Avance III HD-600 spectrometer [600 (¹H) and 150 MHz (¹³C)], a Bruker Avance 400 spectrometer [400 (¹H) and 100 MHz (¹³C)], or a Bruker Avance 250 spectrometer [250 (¹H) and 63 MHz (¹³C)]; chemical shifts are reported relative to the residual solvent peak. The circular dichroism spectra were recorded with a JASCO J-815 spectropolarimeter equipped with a 150 W xenon lamp. The ellipticity was obtained by calibrating the instruments with a 0.06% (w/v) aqueous solution of ammonium D-10-camphorsulfonate and with a 0.08% (w/v) aqueous solution of tris(ethylenediamine)cobalt(III) chloride complex {(-)-Δ-[Co(en)₃]-Cl₃}₂·NaCl·6H₂O. The measurements were performed at a constant temperature of 25 °C in quartz cells and were corrected for the contribution from the cell and solvent. The temperature was controlled by a Jasco PTC-423S/15 Peltier-type temperature control system cooled with an external water circulator. The spectra were corrected to take into account the dilution effect after each addition. The HPLC system consisted of a Jasco PU-2089 Plus pump and a Jasco MD-2010 Plus multiwavelength detector. The HPLC column was a Waters Spherisorb® 10 µm CN 10 × 250 mm semipreparative column. Compounds **4**,^[7a] **8**,^[18] and **9**^[35] were synthesized according to literature procedures. Poly(dA)–poly(dT) sodium salt was purchased from Sigma–Aldrich. Water was purified through a Millipore Milli-Q system. All CD experiments were conducted in 10⁻² M phosphate buffer at pH = 7.4 containing 0.1 M NaCl. The pH of the solution was measured with a glass electrode. The concentrations of polynucleotides in base pairs were determined by absorption spectroscopy by using the molar extinction coefficient 12000 M⁻¹ cm⁻¹ at 260 nm.

Synthesis of 5a–7a: Compound **9** (0.105 g, 0.147 mmol) and (±)-**4a** (0.233 g, 0.735 mmol) were dissolved in dry CH₂Cl₂ (15 mL), and then dry Et₃N (0.101 mL, 0.735 mmol) was added. The reaction

mixture was stirred at room temperature for 48 h. Then, the mixture was washed twice with H_2O , the organic phase was dried with Na_2SO_4 , and the solvent was removed under reduced pressure. The products were isolated by silica gel flash column chromatography ($\text{CH}_2\text{Cl}_2/\text{Et}_2\text{O}$, 96:4). Compounds (\pm) -**6a** and **7a** were purified by HPLC (mobile phase: hexane/isopropyl alcohol, 80:20, v/v; flow rate 1.6 mL/min).

Compound (\pm) -5a: 22 mg, 15% yield. ESI(+) MS: m/z = 981.7 [$\text{M} + \text{H}]^+$, 1003.1 [$\text{M} + \text{Na}]^+$. M.p. >200 °C (dec.). ^1H NMR (400 MHz, CDCl_3 , 298 K): δ = 0.97–1.01 (overlapped, 12 H, $\text{OCH}_2\text{CH}_2\text{CH}_3$), 1.87–1.96 (overlapped, 8 H, $\text{OCH}_2\text{CH}_2\text{CH}_3$), 2.66 and 2.83 (br. AB, 2 H, $\text{CH}_2^{\text{isox}}$), 2.78 (br. s, 3 H, CH_3N), 3.18–3.26 (overlapped, 4 H, ArCH_2Ar), 3.80–3.85 (overlapped, 4 H, $\text{OCH}_2\text{CH}_2\text{CH}_3$), 3.90–3.96 (overlapped, 4 H, $\text{OCH}_2\text{CH}_2\text{CH}_3$), 4.41–4.48 (overlapped, 4 H, ArCH_2Ar), 4.45 and 4.56 [AB, 2 H, $\text{C}(\text{O})\text{OCH}_2^{\text{isox}}$], 4.70 (br. s, 1 H, OCH^{isox}), 4.80 (br. s, 1 H, NCH^{isox}), 6.44–6.62 (overlapped, 6 H, ArH), 7.39 (br. s, 2 H, ArH), 7.50 (br. s, 2 H, ArH), 7.99–8.47 (overlapped, 9 H, $\text{ArH}^{\text{pyrene}}$) ppm. ^{13}C NMR (100 MHz, CDCl_3 , 298 K): δ = 10.30, 10.35, 23.24, 23.33, 29.72, 30.96, 41.77, 44.02, 65.40, 69.30, 75.30, 76.90, 77.24, 122.42, 122.57, 122.81, 123.44, 124.61, 124.81, 124.95, 125.09, 125.38, 126.03, 127.47, 127.89, 128.38, 128.45, 128.53, 128.81, 129.94, 130.23, 130.43, 130.56, 130.64, 130.73, 131.37, 134.20, 134.35, 135.47, 135.60, 156.20, 161.25, 161.54, 166.46, 169.68 ppm. $\text{C}_{84}\text{H}_{82}\text{N}_2\text{O}_{10}$ (1279.6): calcd. C 78.85, H 6.46; found C 78.93, H 6.38.

Compound (\pm) -6a: 19 mg, 10% yield. ESI(+) MS: m/z = 1280.4 [$\text{M} + \text{H}]^+$. M.p. >180 °C (dec.). ^1H NMR (400 MHz, CDCl_3 , 298 K): δ = 0.96 (t, J = 7.4 Hz, 6 H, $\text{OCH}_2\text{CH}_2\text{CH}_3$), 1.01 (t, J = 7.3 Hz, 6 H, $\text{OCH}_2\text{CH}_2\text{CH}_3$), 1.83–1.99 (overlapped, 8 H, $\text{OCH}_2\text{CH}_2\text{CH}_3$), 2.68 and 2.87 (br. AB, 4 H, $\text{CH}_2^{\text{isox}}$), 2.80 (br. s, 6 H, CH_3N), 3.20 and 4.44 (AX, J = 13.2 Hz, 4 H, ArCH_2Ar), 3.25 and 4.46 (AX, J = 13.2 Hz, 4 H, ArCH_2Ar), 3.75 (t, J = 6.8 Hz, 4 H, $\text{OCH}_2\text{CH}_2\text{CH}_3$) 4.02 (t, J = 7.6 Hz, 4 H, $\text{OCH}_2\text{CH}_2\text{CH}_3$), 4.58 and 4.50 [AB, 4 H, $\text{C}(\text{O})\text{OCH}_2^{\text{isox}}$], 4.76 (br. s, 2 H, OCH^{isox} and 2 H, NCH^{isox}), 6.22 (br. s, 4 H, ArH), 6.37 (br. s, 2 H, ArH), 7.65 (br. s, 2 H, ArH), 7.67 (br. s, 2 H, ArH), 7.98–8.49 (overlapped, 18 H, $\text{ArH}^{\text{pyrene}}$) ppm. ^{13}C NMR (100 MHz, CDCl_3 , 298 K): δ = 10.15, 10.53, 23.28, 23.35, 30.95, 41.96, 44.14, 65.34, 69.24, 75.10, 76.7, 76.9, 122.36, 122.63, 123.30, 124.46, 124.82, 124.97, 125.06, 125.37, 126.03, 127.41, 127.48, 127.86, 128.14, 130.26, 130.39, 130.65, 130.70, 131.39, 133.57, 136.23, 155.76, 161.82, 166.47 ppm. $\text{C}_{84}\text{H}_{82}\text{N}_2\text{O}_{10}$ (1279.6): calcd. C 78.85, H 6.46; found C 78.95, H 6.36.

Compound 7a: 15 mg, 8% yield. ESI(+) MS: m/z = 1280.4 [$\text{M} + \text{H}]^+$. M.p. >170 °C (dec.). ^1H NMR (400 MHz, C_6D_6 , 298 K): δ = 0.84–0.91 (overlapped, 12 H, $\text{OCH}_2\text{CH}_2\text{CH}_3$), 1.73–1.86 (overlapped, 8 H, $\text{OCH}_2\text{CH}_2\text{CH}_3$), 2.44 and 2.72 (br. AB, 4 H, $\text{CH}_2^{\text{isox}}$), 2.73 (br. s, 6 H, CH_3N), 3.07 and 4.39 (AX, J = 13.2 Hz, 4 H, ArCH_2Ar), 3.14 and 4.45 (AX, J = 13.6 Hz, 4 H, ArCH_2Ar), 3.65 (t, J = 7.2 Hz, 2 H, $\text{OCH}_2\text{CH}_2\text{CH}_3$), 3.70 (t, J = 7.6 Hz, 2 H, $\text{OCH}_2\text{CH}_2\text{CH}_3$), 3.86 (t, J = 7.2 Hz, 4 H, $\text{OCH}_2\text{CH}_2\text{CH}_3$), 4.54–4.69 [overlapped, 8 H, $\text{C}(\text{O})\text{OCH}_2^{\text{isox}}$, OCH, NCH], 6.25 (t, J = 7.4 Hz, 2 H, ArH), 6.41 (d, J = 7.4 Hz, 2 H, ArH), 6.64 (d, J = 6.9 Hz, 2 H, ArH), 7.76–8.00 (overlapped, 22 H, $\text{ArH}^{\text{pyrene}}$) ppm. ^1H NMR (400 MHz, CDCl_3 , 298 K): δ = 0.96 (t, J = 7.4 Hz, 6 H, $\text{OCH}_2\text{CH}_2\text{CH}_3$), 1.01–1.06 (overlapped, 6 H, $\text{OCH}_2\text{CH}_2\text{CH}_3$), 1.85–1.99 (overlapped, 8 H, $\text{OCH}_2\text{CH}_2\text{CH}_3$), 2.66 and 2.85 (br. AB, 4 H, $\text{CH}_2^{\text{isox}}$), 2.79 (br. s, 6 H, CH_3N), 3.23 (d, J = 13.6 Hz, 2 H, ArCH_2Ar), 3.27 (d, J = 13.8 Hz, 2 H, ArCH_2Ar), 3.72–3.78 (overlapped, 4 H, $\text{OCH}_2\text{CH}_2\text{CH}_3$), 4.04 (t, J = 7.2 Hz, 4 H, $\text{OCH}_2\text{CH}_2\text{CH}_3$), 4.44–4.52 (overlapped, 4 H, ArCH_2Ar), 4.57 and 4.50 [AB, 4 H, $\text{C}(\text{O})\text{OCH}_2^{\text{isox}}$], 4.76 (br. s, 2 H, OCH, and 2 H,

NCH), 6.20–6.38 (overlapped, 6 H, ArH), 7.70 (br. s, 4 H, ArH), 7.98–4.49 (overlapped, 18 H, $\text{ArH}^{\text{pyrene}}$) ppm. ^{13}C NMR (63 MHz, CDCl_3 , 298 K): δ = 10.12, 10.57, 23.27, 23.37, 30.99, 41.77, 44.04, 65.28, 69.22, 75.12, 76.82, 77.23, 122.40, 122.60, 123.29, 124.51, 124.81, 124.96, 125.07, 125.37, 126.02, 127.47, 127.85, 128.11, 128.83, 130.31, 130.41, 130.63, 130.70, 131.37, 133.47, 136.33, 155.86, 155.90, 162.12, 166.70 ppm. $\text{C}_{84}\text{H}_{82}\text{N}_2\text{O}_{10}$ (1279.6): calcd. C 78.85, H 6.46; found C 78.93, H 6.38.

Synthesis of Compounds 5b and 6b: Compound **9** (0.210 g, 0.29 mmol) and (\pm) -**4b** (0.206 g, 0.65 mmol) were dissolved in dry pyridine (5 mL). The reaction mixture was stirred at room temperature for 24 h, and then the solvent was removed under reduced pressure. The pure products were isolated by flash column chromatography with silica gel ($\text{CH}_2\text{Cl}_2/\text{Et}_2\text{O}$, 98:2).

Compound (\pm) -5b: 28 mg, 10% yield. ESI(+) MS: m/z = 981.0 [$\text{M} + \text{H}]^+$. M.p. >200 °C (dec.). ^1H NMR (250 MHz, CDCl_3 , 298 K): δ = 0.94–1.05 (overlapped, 12 H, $\text{OCH}_2\text{CH}_2\text{CH}_3$), 1.86–1.94 (overlapped, 8 H, $\text{OCH}_2\text{CH}_2\text{CH}_3$), 2.28–2.41 (br. m, 1 H, $\text{CH}_2^{\text{isox}}$), 2.73 (s, 3 H, CH_3N), 3.08–3.23 (overlapped, 1 H, ArCH_2Ar and 4 H, $\text{CH}_2^{\text{isox}}$), 3.82–3.89 (overlapped, 8 H, $\text{OCH}_2\text{CH}_2\text{CH}_3$), 4.23–4.53 [overlapped, 2 H, ArCH_2Ar and 4 H, $\text{C}(\text{O})\text{OCH}_2^{\text{isox}}$], 4.66–4.72 (overlapped, 1 H, OCH and 1 H, NCH), 6.60–6.74 (overlapped, 6 H, ArH), 7.20 (s, 2 H, ArH), 7.36 (s, 2 H, ArH), 7.99–8.38 (overlapped, 9 H, $\text{ArH}^{\text{pyrene}}$) ppm. ^{13}C NMR (63 MHz, CDCl_3 , 298 K): δ = 10.24, 10.36, 10.39, 22.71, 23.18, 23.32, 29.71, 30.32, 30.90, 41.06, 43.43, 65.95, 69.22, 76.72, 77.22, 122.18, 122.43, 122.92, 123.64, 123.95, 124.17, 124.82, 124.94, 125.08, 125.41, 125.45, 126.03, 127.40, 127.90, 128.60, 128.71, 128.83, 129.85, 130.04, 130.18, 130.27, 130.61, 130.65, 131.37, 132.53, 134.59, 134.96, 135.09, 135.31, 156.45, 156.64, 160.82, 161.03, 166.69 ppm. $\text{C}_{63}\text{H}_{65}\text{NO}_9$ (980.2): calcd. C 77.20, H 6.68; found C 77.29, H 6.59.

Compound (\pm) -6b: 41 mg, 11% yield. ESI(+) MS: m/z = 1280.4 [$\text{M} + \text{H}]^+$. M.p. >170 °C (dec.). ^1H NMR (400 MHz, CDCl_3 , 298 K): δ = 0.91 (t, J = 7.4 Hz, 6 H, $\text{OCH}_2\text{CH}_2\text{CH}_3$), 1.07 (t, J = 7.3 Hz, 6 H, $\text{OCH}_2\text{CH}_2\text{CH}_3$), 1.84–1.97 (overlapped, 8 H, $\text{OCH}_2\text{CH}_2\text{CH}_3$), 2.31 and 3.20 (br. AX, 4 H, $\text{CH}_2^{\text{isox}}$), 2.79 (br. s, 6 H, CH_3N), 3.16–3.22 (overlapped, 4 H, ArCH_2Ar), 3.69 (t, J = 6.3 Hz, 4 H, $\text{OCH}_2\text{CH}_2\text{CH}_3$) 4.04 (t, J = 7.6 Hz, 4 H, $\text{OCH}_2\text{CH}_2\text{CH}_3$), 4.39–4.44 (overlapped, 4 H, ArCH_2Ar), 4.42 and 4.62 [AB, 4 H, $\text{C}(\text{O})\text{OCH}_2^{\text{isox}}$], 4.72 (br. s, 2 H, NCH^{isox}), 4.79 (br. s, 2 H, OCH^{isox}), 6.13–6.21 (overlapped, 6 H, ArH), 7.73 (br. s, 4 H, ArH), 7.99–8.42 (overlapped, 18 H, $\text{ArH}^{\text{pyrene}}$) ppm. ^{13}C NMR (150 MHz, CDCl_3 , 298 K): δ = 9.98, 10.72, 23.17, 23.46, 30.86, 42.21, 43.73, 66.46, 69.12, 74.84, 122.33, 122.40, 123.32, 124.20, 124.85, 124.95, 125.08, 125.36, 125.49, 126.01, 127.32, 127.49, 127.85, 128.68, 130.52, 130.60, 130.65, 131.38, 132.88, 132.93, 133.17, 136.64, 155.32, 162.24, 166.78 ppm. $\text{C}_{84}\text{H}_{82}\text{N}_2\text{O}_{10}$ (1279.6): calcd. C 78.85, H 6.46; found C 78.95, H 6.36.

Cell Viability Assays: FTC133, 8305C, and U87MG cell lines were seeded in 96-well plates. The cells were grown in an appropriate medium supplemented with 10% fetal bovine serum and incubated at 37 °C, 5% CO_2 conditions, for 24 h before the cytotoxicity assessments. The cells were exposed to increased concentrations of the compounds. After 24 h of incubation, the cell survival was determined by MTT assay according to the literature procedure.^[36] In brief, MTT solution [50 μL , 5 mg/mL in phosphate-buffered saline (PBS), Sigma] was added to each well and incubated for 2 h. The medium was subsequently removed from the wells, and the resulting formazan crystals were dissolved in DMSO (100 μL). The culture plates were rocked gently for 30 min to dissolve the crystals before the optical density was measured at 570 nm with an enzyme-linked immunosorbent assay (ELISA) microplate reader. In all ex-

periments, four replicate wells were measured for each drug concentration.

Molecular Modeling

Preparation of Ligands: The 3D structures of the ligands were generated with the Winmostar (4.101) software,^[37] and all geometries were fully optimized with the same software with the semiempirical AM1^[38] Hamiltonian implemented in MOPAC2012 (14.04W).^[39] Compounds **5** were optimized as carboxylates (charge = -1).

Molecular Dynamics Simulations: The molecular dynamics simulations of the DNA–ligand complexes were performed with the YASARA structure package (13.9.8).^[28] A periodic simulation cell with boundaries extending 10 Å from the surface of the complex was employed. The box was filled with water, and a density of 0.997 g/mL with explicit solvent was utilized. The pK_a utility of YASARA was used to assign pK_a values at pH = 7.2,^[40] the cell was neutralized with 22 Na⁺ ions (23 for **5**), and NaCl was added to reach 0.9% concentration by mass; under these conditions, ligands **5** were deprotonated at the carboxylic acid function. Water molecules were deleted to readjust the solvent density to 0.997 g/mL. The Amber03 force field was used with long-range electrostatic potentials calculated with the particle mesh Ewald (PME) method with a cutoff of 7.86 Å.^[29,41] The ligand force-field parameters were generated with the AutoSMILES utility,^[42] which employs semiempirical AM1 geometry optimization and assignment of charges, followed by assignment of the AM1BCC atom and bond types with refinement by using the restrained electrostatic potential (RESP) charges, and finally the assignments of general AMBER force field atom types. A short MD simulation was run for the solvent only. The entire system was then energy-minimized through a steepest-descent minimization to remove conformational stress, followed by a simulated annealing minimization until convergence (<0.01 kcal/mol Å). The MD simulation was then initiated; the *NVT* ensemble at 298 K was used, and the time steps for intramolecular and intermolecular forces were integrated every 1.25 and 2.5 fs, respectively. The MD simulation was stopped after 5 ns and, on the last frame, a second cycle of energy minimization, identical to the first, was applied.

Docking Protocol: The DNA–ligand complexes, as obtained after coarse minimization or MD simulation and energy minimization, were prepared with Vega ZZ^[43] (3.0.3.18) with Gasteiger charges assigned to the proteins and AM1BCC ones assigned to the ligands. The graphical user interface AutoDockTools (1.5.7 rc1)^[44] was used to establish the Autogrid points and to visualize the docked ligand–nucleic acid structures. Docking was performed with the AutoDock (4.2.5.1) software.^[32] To define all binding sites and to have structural inputs, a grid-based procedure was used.^[45] Here, the output was saved as a PDBQT file. The grid box was set, and the output was saved as a gpf file. The ligand-centered maps were generated by the program AutoGrid (4.2.5.1) with a spacing of 0.375 Å and dimensions that encompass all atoms extending 10 Å from the surface of the ligand (for blind docking, DNA-centered maps were generated with a spacing of 0.375 Å and dimensions that encompass all atoms extending 10 Å from the surface of DNA). All of the parameters were inserted at their default settings. In the docking tab, the macromolecule and ligand were selected, and the GA parameters were set as ga_runs = 100, ga_pop_size = 150, ga_num_evals = 2500000 for coarse docking and 20000000 for fine docking, ga_num_generations = 27000, ga_elitism = 1, ga_mutation_rate = 0.02, ga_crossover_rate = 0.8, ga_crossover_mode = two points, ga_cauchy_alpha = 0.0, ga_cauchy_beta = 1.0, number of generations for picking worst individual = 10, output was selected as LGA, and the file was saved as a dpf file.

Circular Dichroism: The CD spectra were recorded with samples in a standard quartz cell of 1 cm path length in the 235–400 nm range. For each spectrum, five runs were averaged with a 5 min equilibration interval before each scan. All spectra were recorded at fixed poly(dA)–poly(dT) concentration (19.7 μM in base pair) in the absence or in the presence of different concentrations of **5b** (4.3 mM solution in DMSO) from 0 to ca. 32 μM.

Supporting Information (see footnote on the first page of this article): ¹H NMR, ¹³C NMR, 2D COSY, 2D HSQC, and ESI(+) mass spectra.

Acknowledgments

The authors thank the Italian Ministero dell'Università e della Ricerca (MIUR) (PRIN 20109Z2XRJ_003 and 20109Z2XRJ_006) for financial support and the Centro di Tecnologie Integrate per la Salute, Università di Salerno (project number PONa3_00138) for the 600 MHz NMR instrument time. Thanks are due to Dr. Patrizia Oliva and Dr. Patrizia Iannece for the NMR spectroscopy and ESI-MS measurements, respectively.

- [1] J. Y. Zhao, W. Li, R. Ma, S. P. Chen, S. M. Ren, T. Jiang, *Int. J. Mol. Sci.* **2013**, *14*, 16851–16865.
- [2] J. B. Chaires, *Curr. Opin. Struct. Biol.* **1998**, *8*, 314–320.
- [3] A. Rescifina, C. Zagni, M. G. Varrica, V. Pistara, A. Corsaro, *Eur. J. Med. Chem.* **2014**, *74*, 95–115.
- [4] a) Y. Chu, *Ph. D. Dissertation, DNA threading intercalation: building sequence-specific linear rigidified and cyclic bisintercalators*, **2007**; <http://hdl.handle.net/2152/3174>; b) M. F. Brana, M. Cacho, A. Gradiñas, B. de Pascual-Teresa, A. Ramos, *Curr. Pharm. Des.* **2001**, *7*, 1745–1780.
- [5] a) L. P. G. Wakelin, *Med. Res. Rev.* **1986**, *6*, 275–340; b) W. M. Cholody, L. Hernandez, L. Hassner, D. A. Scudiero, D. B. Djurickovic, C. J. Michejda, *J. Med. Chem.* **1995**, *38*, 3043–3052.
- [6] P. F. Bousquet, M. F. Brana, D. Conlon, K. M. Fitzgerald, D. Perron, C. Cocchiaro, R. Miller, M. Moran, J. George, X. D. Qian, G. Keilhauer, C. A. Romerdahl, *Cancer Res.* **1995**, *55*, 1176–1180.
- [7] a) A. Rescifina, M. A. Chiacchio, A. Corsaro, E. De Clercq, D. Iannazzo, A. Mastino, A. Piperno, G. Romeo, R. Romeo, V. Valveri, *J. Med. Chem.* **2006**, *49*, 709–715; b) A. Rescifina, U. Chiacchio, A. Piperno, S. Sortino, *New J. Chem.* **2006**, *30*, 554–561; c) A. Rescifina, U. Chiacchio, A. Corsaro, A. Piperno, R. Romeo, *Eur. J. Med. Chem.* **2011**, *46*, 129–136; d) A. Rescifina, M. G. Varrica, C. Carnovale, G. Romeo, U. Chiacchio, *Eur. J. Med. Chem.* **2012**, *51*, 163–173; e) A. Rescifina, C. Zagni, G. Romeo, S. Sortino, *Bioorg. Med. Chem.* **2012**, *20*, 4978–4984.
- [8] C. D. Gutsche, *Calixarenes: An Introduction*, 2nd ed., RSC Publishing, Cambridge, UK, **2008**.
- [9] a) I. Columbus, S. E. Biali, *Org. Lett.* **2007**, *9*, 2927–2929; b) K. Kogan, S. E. Biali, *Org. Lett.* **2007**, *9*, 2393–2396; c) C. Gaeta, F. Troisi, M. Martino, E. Gavuzzo, P. Neri, *Org. Lett.* **2004**, *6*, 3027–3030; d) F. Troisi, T. Pierro, C. Gaeta, M. Carratù, P. Neri, *Tetrahedron Lett.* **2009**, *50*, 4416–4419; e) F. Troisi, T. Pierro, C. Gaeta, P. Neri, *Org. Lett.* **2009**, *11*, 697–700.
- [10] a) L. Baldini, A. Casnati, F. Sansone, R. Ungaro, *Chem. Soc. Rev.* **2007**, *36*, 254–266; b) A. Casnati, F. Sansone, R. Ungaro, *Acc. Chem. Res.* **2003**, *36*, 246–254; c) M. W. Peczu, A. D. Hamilton, *Chem. Rev.* **2000**, *100*, 2479–2493.
- [11] a) S. Cherenok, A. Vovk, I. Muravyova, A. Shivanuk, V. Kukhar, J. Lipkowski, V. Kalchenko, *Org. Lett.* **2006**, *8*, 549–552; b) M. G. Chini, S. Terracciano, R. Riccio, G. Bifulco, R. Ciao, C. Gaeta, F. Troisi, P. Neri, *Org. Lett.* **2010**, *12*, 5382–5385; c) S. Francese, A. Cozzolino, L. Caputo, C. Esposito, M. Martino, C. Gaeta, F. Troisi, P. Neri, *Tetrahedron Lett.* **2005**, *46*, 1611–1615; d) T. Mecca, G. M. L. Consoli, C. Geraci, F. Cun-

- solo, *Bioorg. Med. Chem.* **2004**, *12*, 5057–5062; e) H. S. Park, Q. Lin, A. D. Hamilton, *J. Am. Chem. Soc.* **1999**, *121*, 8–13; f) H. S. Park, Q. Lin, A. D. Hamilton, *Proc. Natl. Acad. Sci. USA* **2002**, *99*, 5105–5109.
- [12] M. A. Blaskovich, Q. Lin, F. L. Delarue, J. Sun, H. S. Park, D. Coppola, A. D. Hamilton, S. M. Sebti, *Nat. Biotechnol.* **2000**, *18*, 1065–1070.
- [13] S. Gordo, V. Martos, E. Santos, M. Menendez, C. Bo, E. Giralt, J. de Mendoza, *Proc. Natl. Acad. Sci. USA* **2008**, *105*, 16426–16431.
- [14] a) S. N. Gradl, J. P. Felix, E. Y. Isacoff, M. L. Garcia, D. Trauner, *J. Am. Chem. Soc.* **2003**, *125*, 12668–12669; b) V. Martos, S. C. Bell, E. Santos, E. Y. Isacoff, D. Trauner, J. de Mendoza, *Proc. Natl. Acad. Sci. USA* **2009**, *106*, 10482–10486.
- [15] a) R. Zadmard, T. Schrader, *Angew. Chem. Int. Ed.* **2006**, *45*, 2703–2706; *Angew. Chem.* **2006**, *118*, 2769; b) W. B. Hu, C. Blecking, M. Kralj, L. Suman, I. Piantanida, T. Schrader, *Chem. Eur. J.* **2012**, *18*, 3589–3597.
- [16] a) V. Bagnacani, F. Sansone, G. Donofrio, L. Baldini, A. Casnati, R. Ungaro, *Org. Lett.* **2008**, *10*, 3953–3956; b) F. Sansone, M. Dedic, G. Donofrio, C. Rivetti, L. Baldini, A. Casnati, S. Cellai, R. Ungaro, *J. Am. Chem. Soc.* **2006**, *128*, 14528–14536.
- [17] M. S. Peters, M. Li, T. Schrader, *Nat. Prod. Commun.* **2012**, *7*, 409–417.
- [18] F. Sansone, S. Barboso, A. Casnati, M. Fabbri, A. Pochini, F. Ugozzoli, R. Ungaro, *Eur. J. Org. Chem.* **1998**, 897–905.
- [19] H. M. Shapiro, *Practical Flow Cytometry*, 4th ed., Wiley, New York, **2003**.
- [20] V. I. Ivanov, L. E. Minchenkova, A. K. Schyolkina, A. I. Poletayev, *Biopolymers* **1973**, *12*, 89–110.
- [21] J. P. Macquet, J. L. Butour, *Eur. J. Biochem.* **1978**, *83*, 375–385.
- [22] L. D. Williams, M. Egli, Q. Gao, A. Rich, *DNA Intercalation: Helix Unwinding and Neighbor-Exclusion*, in: *Structure & Function: Proceedings of the Seventh Conversation in Biomolecular Stereodynamics*, Adenine Press, Schenectady, **1992**, pp. 107–125.
- [23] S. Kashanian, N. Shahabadi, H. Roshanfekr, K. Shalmashi, K. Omidfar, *Biochemistry (Moscow)* **2008**, *73*, 929–936.
- [24] a) X. Y. Xu, D. D. Wang, X. J. Sun, S. Y. Zeng, L. W. Li, D. Z. Sun, *Thermochim. Acta* **2009**, *493*, 30–36; b) G. W. Zhang, P. Fu, L. Wang, M. M. Hu, *J. Agric. Food Chem.* **2011**, *59*, 8944–8952; c) E. Grueso, G. López-Pérez, M. Castellano, R. Prado-Gotor, *J. Inorg. Biochem.* **2012**, *106*, 1–9; d) S. Kashanian, M. M. Khodaei, H. Roshanfekr, N. Shahabadi, G. Mansouri, *Spectrochim. Acta Part A* **2012**, *86*, 351–359; e) M. A. Nazif, R. Rubbiani, H. Alborzinia, I. Kitanovic, S. Wolf, I. Ott, W. S. Sheldrick, *Dalton Trans.* **2012**, *41*, 5587–5598; f) N. Shahabadi, N. H. Moghadam, *Spectrochim. Acta Part A* **2012**, *99*, 18–22; g) G. W. Zhang, X. Hu, P. Fu, *J. Photochem. Photobiol. B: Biology* **2012**, *108*, 53–61; h) K. Benner, A. Bergen, H. Ihmels, P. M. Pithan, *Chem. Eur. J.* **2014**, *20*, 9883–9887; i) Y. D. Ma, G. W. Zhang, J. H. Pan, *J. Agric. Food Chem.* **2012**, *60*, 10867–10875; j) S. Mahadevan, M. Palaniandavar, *Inorg. Chem.* **1998**, *37*, 693–700; k) M. Shaghaghi, G. Dehghan, A. Jouyban, P. Sistani, M. Arvin, *Spectrochim. Acta Part A* **2014**, *120*, 467–472.
- [25] a) S. Parodi, F. Kendall, C. Nicolini, *Nucleic Acids Res.* **1975**, *2*, 477–486; b) Y. M. Chang, C. K. M. Chen, M. H. Hou, *Int. J. Mol. Sci.* **2012**, *13*, 3394–3413.
- [26] a) E. Grueso, R. Prado-Gotor, *Chem. Phys.* **2010**, *373*, 186–192; b) F. Secco, M. Venturini, T. Biver, F. Sánchez, R. Prado-Gotor, E. Grueso, *J. Phys. Chem. B* **2010**, *114*, 4686–4691.
- [27] R. Lyng, T. Hard, B. Norden, *Biopolymers* **1987**, *26*, 1327–1345.
- [28] E. Krieger, *YASARA*, 13.9.8 ed., YASARA Biosciences GmbH, Vienna, **2013**.
- [29] Y. Duan, C. Wu, S. Chowdhury, M. C. Lee, G. M. Xiong, W. Zhang, R. Yang, P. Cieplak, R. Luo, T. Lee, J. Caldwell, J. M. Wang, P. Kollman, *J. Comput. Chem.* **2003**, *24*, 1999–2012.
- [30] C. G. Ricci, A. S. C. de Andrade, M. Mottin, P. A. Netz, *J. Phys. Chem. B* **2010**, *114*, 9882–9893.
- [31] O. A. Santos-Filho, J. D. Figueiroa-Villar, M. T. Araujo, *Bioorg. Med. Chem. Lett.* **1997**, *7*, 1797–1802.
- [32] G. M. Morris, R. Huey, W. Lindstrom, M. F. Sanner, R. K. Belew, D. S. Goodsell, A. J. Olson, *J. Comput. Chem.* **2009**, *30*, 2785–2791.
- [33] P. A. Holt, J. B. Chaires, J. O. Trent, *J. Chem. Inf. Model.* **2008**, *48*, 1602–1615.
- [34] C. Hetenyi, D. van der Spoel, *Protein Sci.* **2002**, *11*, 1729–1737.
- [35] L. Baldini, P. Ballester, A. Casnati, R. M. Gomila, C. A. Hunter, F. Sansone, R. Ungaro, *J. Am. Chem. Soc.* **2003**, *125*, 14181–14189.
- [36] A. J. Pope, C. Bruce, B. Kysela, M. J. Hannon, *Dalton Trans.* **2010**, *39*, 2772–2774.
- [37] N. Senda, *Idemitsu Gihō* **2006**, *49*, 106–111.
- [38] M. J. S. Dewar, E. G. Zoebisch, E. F. Healy, J. J. P. Stewart, *J. Am. Chem. Soc.* **1985**, *107*, 3902–3909.
- [39] J. J. P. Stewart, *MOPAC*, Stewart Computational Chemistry, Colorado Springs, **2012**.
- [40] E. Krieger, J. E. Nielsen, C. A. E. M. Spronk, G. Vriend, *J. Mol. Graphics Modell.* **2006**, *25*, 481–486.
- [41] a) W. D. Cornell, P. Cieplak, C. I. Bayly, I. R. Gould, K. M. Merz, D. M. Ferguson, D. C. Spellmeyer, T. Fox, J. W. Caldwell, P. A. Kollman, *J. Am. Chem. Soc.* **1995**, *117*, 5179–5197; b) U. Essmann, L. Perera, M. L. Berkowitz, T. Darden, H. Lee, L. G. Pedersen, *J. Chem. Phys.* **1995**, *103*, 8577–8593.
- [42] A. Jakalian, D. B. Jack, C. I. Bayly, *J. Comput. Chem.* **2002**, *23*, 1623–1641.
- [43] A. Pedretti, L. Villa, G. Vistoli, *J. Comput.-Aided Mol. Des.* **2004**, *18*, 167–173.
- [44] M. F. Sanner, *J. Mol. Graphics Modell.* **1999**, *17*, 57–61.
- [45] P. J. Goodford, *J. Med. Chem.* **1985**, *28*, 849–857.

Received: August 7, 2014

Published Online: October 21, 2014